# Supporting Information

## Covalent triazine frameworks for the selective sorption of palladium from highly acidic radioactive liquid wastes

Pengcheng Wu,[a] Hui Liu,[a] Mengqi Sun,[a] Yaxin Zeng,[a] Jiawei Ye,[b] Song Qin,[a] Yimin Cai,*[a] Wen Feng,*[a] Lihua Yuan

[a.] Key Laboratory of Radiation Physics and Technology of Ministry of Education, Institute of Nuclear Science and Technology, College of Chemistry, Sichuan University, Chengdu, 610064, China; correspondence to: Email: wfeng9510@scu.edu.cn; ymcai@scu.edu.cn.

[b.] Irradiation Preservation Technology Key Laboratory of Sichuan Province, Chengdu 610101, China.

# SUPPORTING INFORMATION

## Contents

1. Synthesis .....3

1.1 Synthesis of 1, 4-Bis (1-imidazolyl) benzene (BIB)[1].....3

1.2 Synthesis of 4, 4'-bis (1-imidazolyl) biphenyl (BIBP)[2].....4

1.3 Synthesis of 2, 4, 6-tris(bromomethyl)-1, 3, 5-triazine (TBT)[3] .....5

1.4 Synthesis of M1 .....6

2. Compound characterization .....7

3. Characterization of CTFs.....12

4. Palladium sorption .....15

5. FT-IR studies of CTFs under different irradiation conditions .....17

6. Sorption mechanism.....18

7. Parameters of kinetics models and isotherm sorption models .....18

8. Comparison of sorption capacity of CTFs with other porous materials .....19

9. Composition of simulated HLLW .....20

References.....21

# SUPPORTING INFORMATION

## 1. Synthesis

1.1 Synthesis of 1, 4-Bis (1-imidazolyl) benzene (BIB)[1]

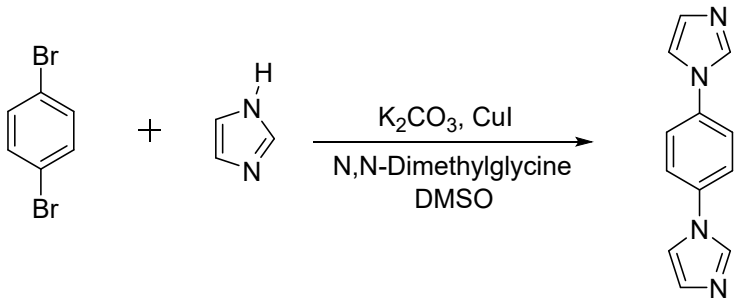


**Scheme S1.** Synthesis of BIB

*N, N*-Dimethylglycine (811 mg, 8.01 mmol), $K_2CO_3$ (11.1 g, 80.1 mmol), 1,4-dibromobenzene (4.71 g, 20.1 mmol), imidazole (3.41 g, 50.1 mmol), and CuI (761 mg, 4.01 mmol) were mixed into a 100 mL round-bottom flask. The flask was evacuated for three times and back filled with Ar, and then dimethyl sulfoxide (50 mL) was added. The reaction mixture was stirred at 110 $^oC$ for 2 days. After being cooled to room temperature, the mixture was poured into 200 mL of ice water. The precipitation was collected by filtration and extracted with $CH_3OH$ (100 mL × 2). The organic phase was dried over anhydrous $MgSO_4$, followed by removing the solvent on a rotary evaporator. The crude product was purfied by column chromatography (silica gel, $CH_2Cl_2/CH_3OH$, 8/1, v/v) to provide the pure product 1,4-Bis(1-imidazolyl)benzene (BIB) as a white power (2.51 g, 59.5%). $^1H$ NMR (400 MHz, $CD_3OD$, 298 K) δ (ppm) 8.23 (t, $J$ = 2.4 Hz, 2 H), 7.77 (s, 4 H), 7.66 (t, $J$ = 1.2 Hz, 2 H), 7.21 (t, $J$ = 2.0 Hz, 2 H).

1.2 Synthesis of 4, 4'-bis (1-imidazolyl) biphenyl (BIBP)[2]

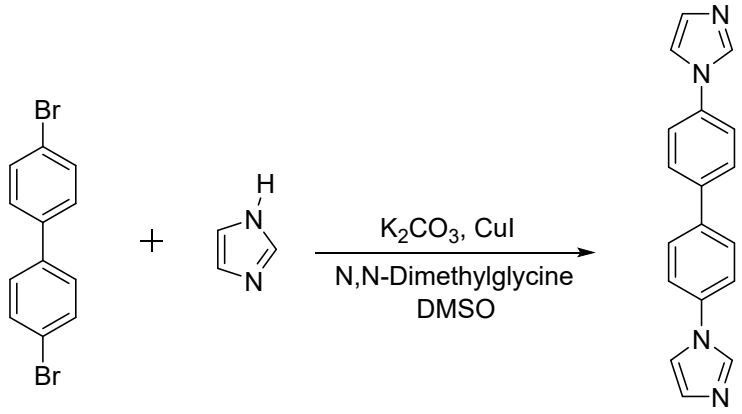


**Scheme S2.** Synthesis of BIBP

The synthetic procedure of 4, 4'-bis(1-imidazolyl)biphenyl (BIBP) is similar with that of BIB. In detail, a mixture of *N, N*-dimethylglycine (810 mg, 8.02 mmol), $K_2CO_3$ (11.1 g, 80.2 mmol), 4,4'-dibromo-1,1'-biphenyl (6.21 g, 20.2 mmol), imidazole (3.41 g, 50.1 mmol), and CuI (762 mg, 4.03 mmol) were added into a 100 mL round-bottom flask. The flask was evacuated for three times and back filled with Ar, and then dimethyl sulfoxide (50 mL) was added. The reaction mixture was stirred at 110 $^oC$ for 2 days. After being cooled to room temperature, the mixture was poured into 200 mL of ice water. The precipitation was collected by filtration and extracted with $CH_3OH$ (100 mL × 2). The organic phase was dried over anhydrous $MgSO_4$, followed by removing the solvent on a rotary evaporator. The crude product was purfied by column chromatography (silica gel, $CH_2Cl_2/CH_3OH$ ,8/1, v/v) to provide the pure product 1,4-Bis(1-imidazolyl)benzene (BIBP)as a white power (4.00 g, 70.2%). $^1H$ NMR (400 MHz, $CD_3OD$, 298 K) δ (ppm) 8.23 (t, $J$ = 2.4 Hz ,2 H), 7.86 (m, 4H), 7.70 (m, 4 H), 7.66 (t, $J$ = 1.2 Hz, 2 H), 7.20 (t, $J$ = 2.8 Hz, 2 H).

1.3 Synthesis of 2, 4, 6-tris(bromomethyl)-1, 3, 5-triazine (TBT)[3]

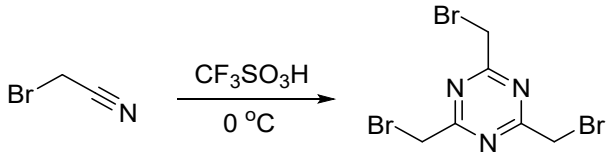


**Scheme S3.** Synthesis of TBT

A solution of triflic acid (40 mL, 448 mmol ) was added dropwise to bromoacetonitrile (15.6 mL, 224 mmol) at 0 °C under $N_2$ atmosphere. After stirring for 12 h, the resulting mixture was added dropwise to a vigorously stirred mixture of $CH_2Cl_2$ (600 mL) and saturated $NaHCO_3$ (aq.) (600 mL). After filteration, the aqueous phase was separated and back extracted with dichloromethane (200 mL). The combined organic layer was washed with brine (200 mL) and dried by $MgSO_4$, followed by removing the solvent under vocuum. The obtained deep red oil was purified by automated flash column chromatography by using a linear gradient of EtOAc into hexane (0–20 %) to give crude product as a brown oil. After recrystallization by adding petroleum ether to chloroform, the pure product was obtained as a white power (6.01 g, 22%). $^1$H NMR (400 MHz, $CDCl_3$, 298 K) δ (ppm) 4.48 (s, 6 H).

1.4 Synthesis of M1

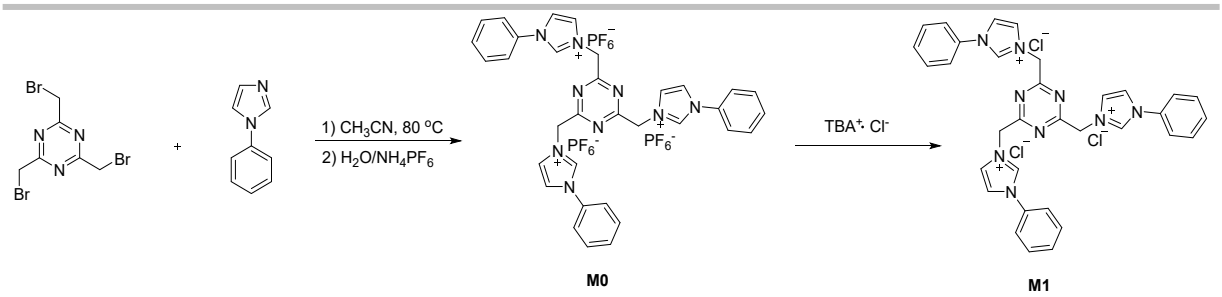


**Scheme S4.** Synthesis of M1

2, 4, 6-tris(bromomethyl)-1, 3, 5-triazine (500 mg, 1.39 mmol) and 1-phenyl-1H-imidazole (1.2 g, 8.34 mmol) were added to 50 mL acetonitrile under $N_2$ atmosphere. After stirring overnight, 30 mL toluene was added into the mixture. The suspension was filtered off and the filtrate was washed with acetontrile (10 mL × 3). The resulting solid was dissolved in water, followed by adding saturated $NH_4^+ \cdot PF_6^-$ solution to the solution. The resulting precipitates were collected by filtration, washed with $H_2O$ (10 mL × 3), and dried at 50 ℃ in a vacuum oven for 5 hours. The water soluble counterparts could be obtained by counterion exchange, which was accomplished by adding $TBA^+ \cdot Cl^-$ into the acetonitrile solution of M0. The pure product was obtained as a brown power by filtration (800 mg, 87.3%). $^1$H NMR (400 MHz, $D_2O$, 298 K) δ (ppm) 7.77 (s, 3 H), 7.63 (s, 3 H ), 7.46-7.38 (m, 15 H), 5.8 (s, 6 H). $^{13}$C NMR (100 MHz,$D_2O$, 298 K) δ (ppm):173.40, 134.00, 130.45, 124.56, 121.39, 52.90. HRMS (ESI) m/z: calcd $[C_{33}H_{30}N_9]^{3+}$ 184.0869, found 184.0865.

## 2. Compound characterization

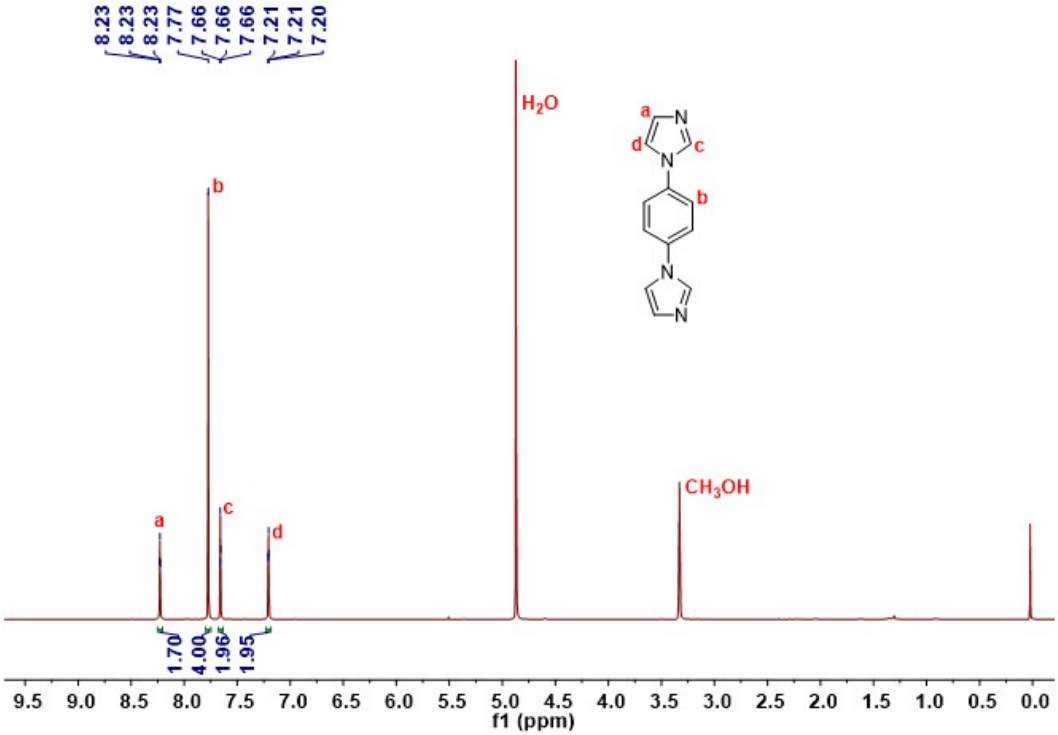


**Fig. S1.** $^{1}$H NMR spectrum (400 MHz, $CD_3OD$, 298 K) of BIB

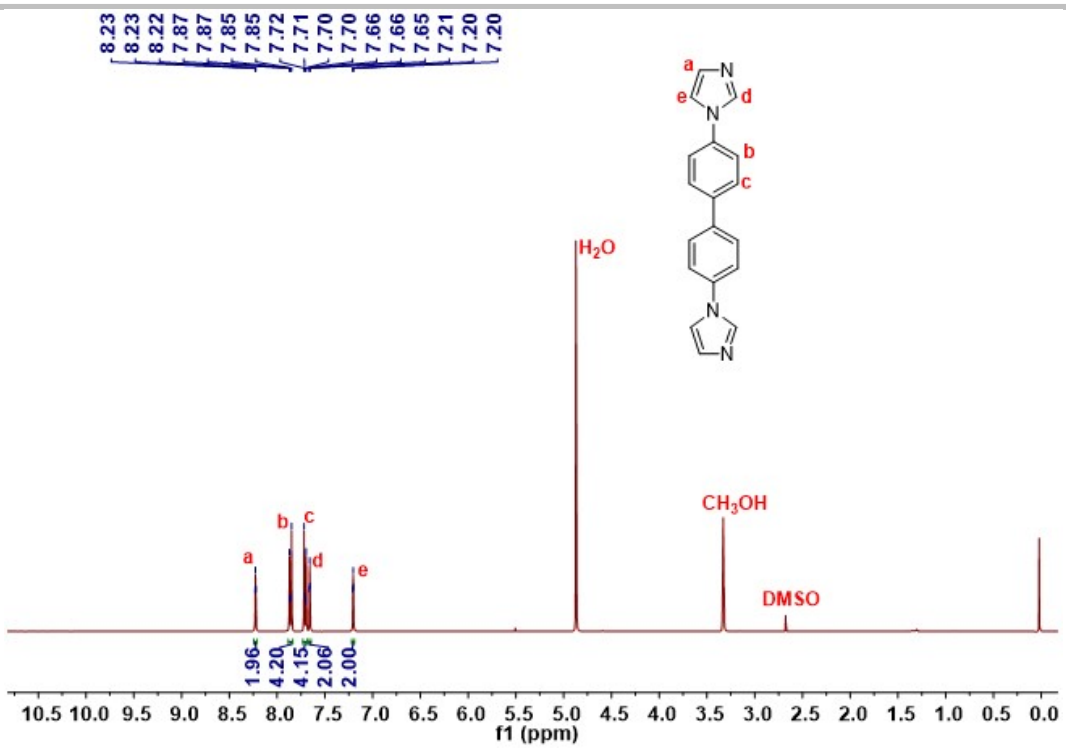


**Fig. S2.** $^{1}$H NMR spectrum (400 MHz, $CD_3OD$, 298 K) of BIBP

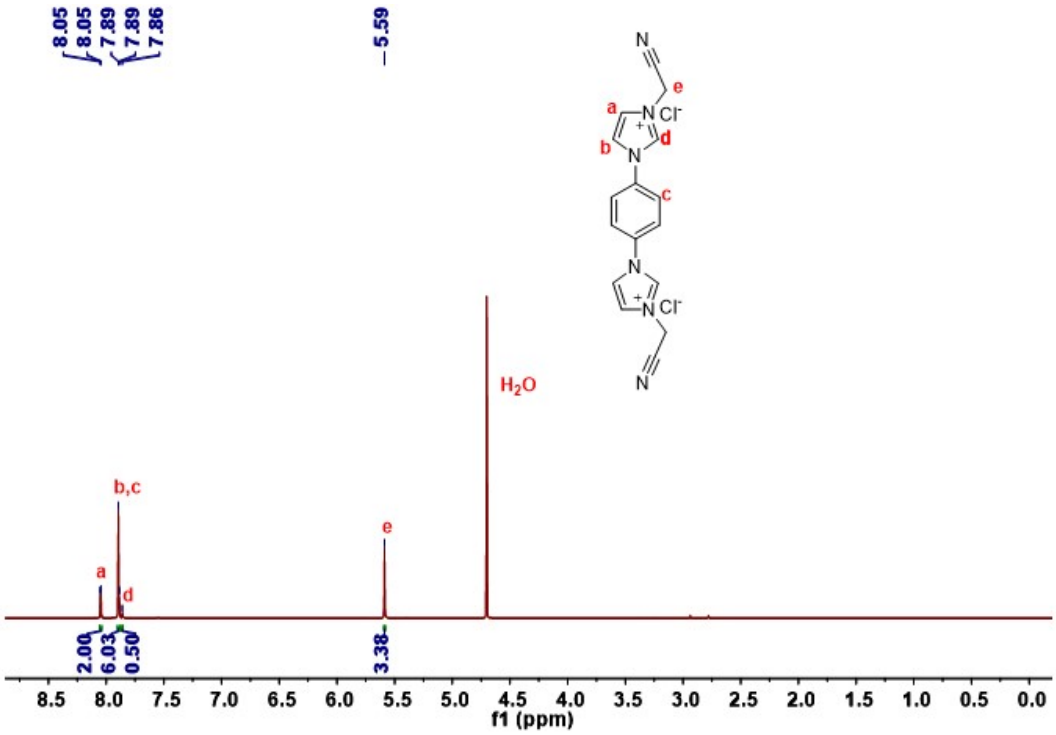


**Fig. S3.** $^{1}$H NMR spectrum (400 MHz, $D_2O$, 298 K) of IL-S

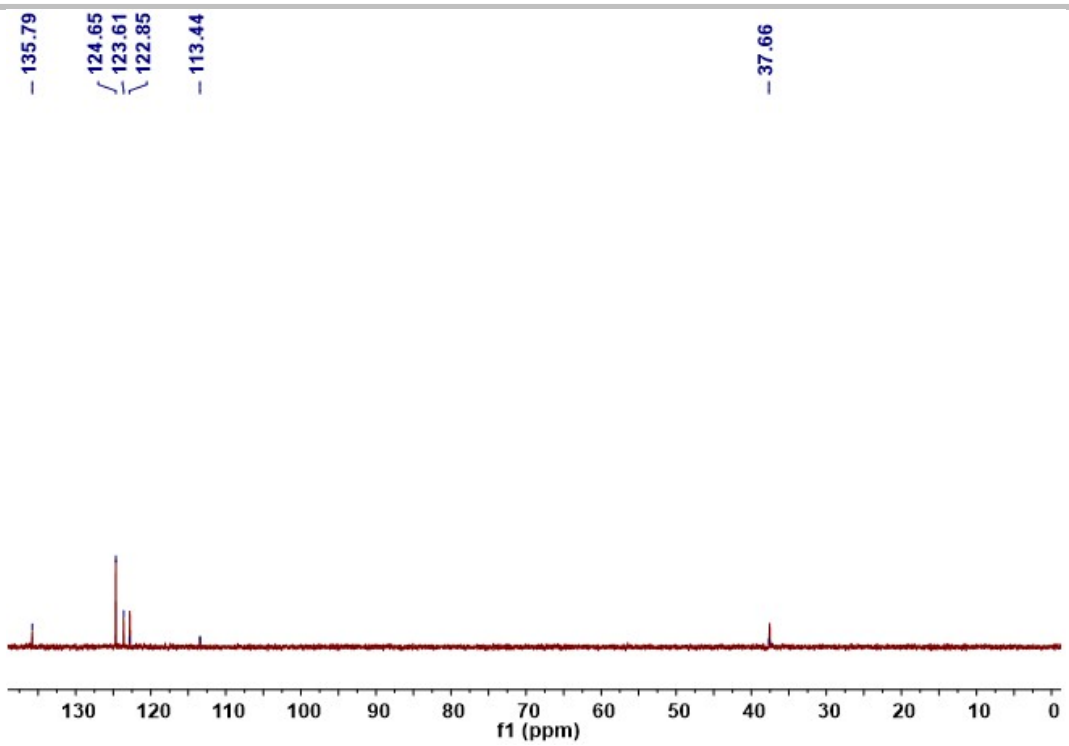


**Fig. S4.** $^{13}$C NMR spectrum (100 MHz, $D_2O$, 298 K) of IL-S

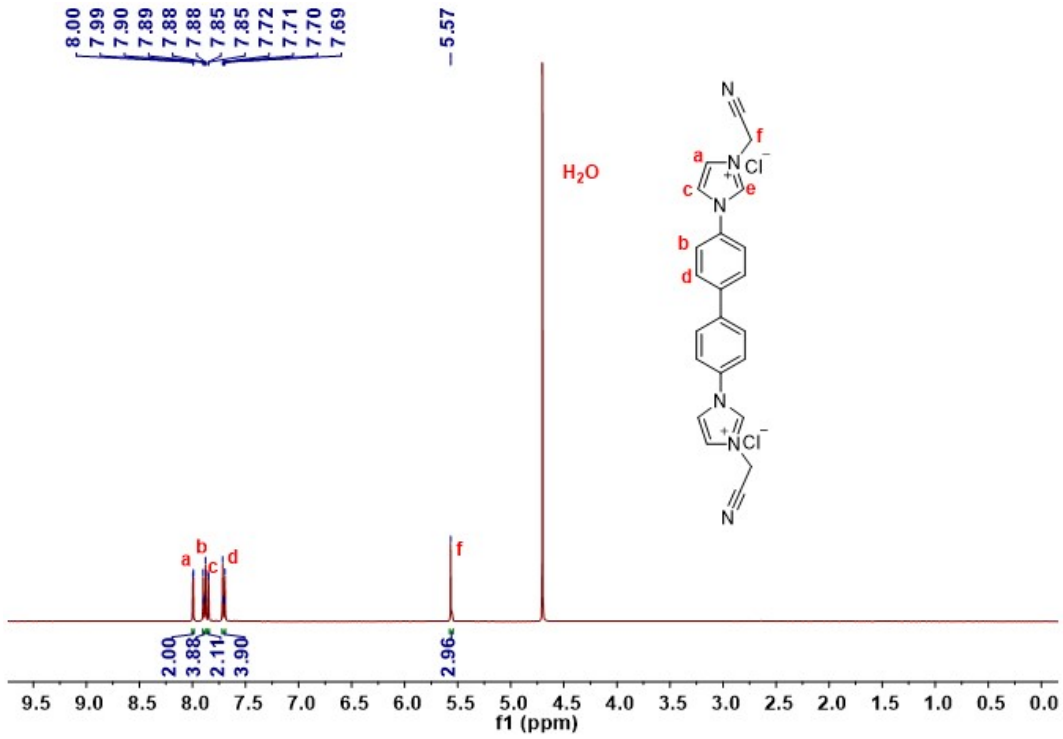


**Fig. S5.** $^{1}$H NMR spectrum (400 MHz, $D_2O$, 298 K) of IL-L

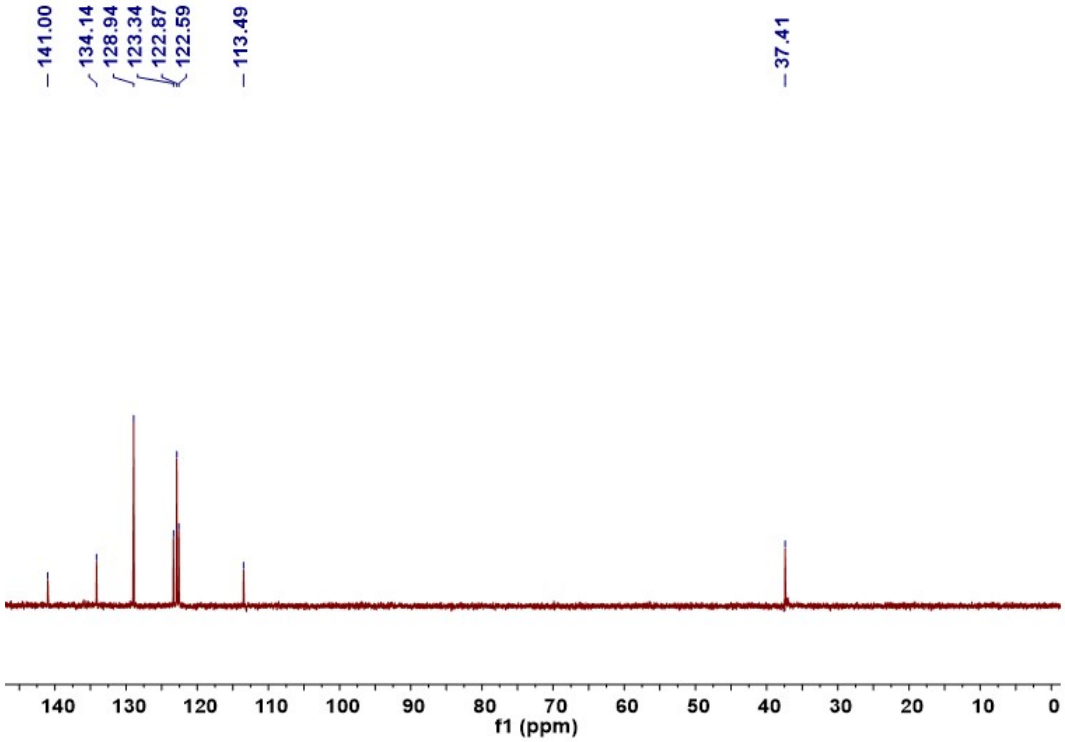


**Fig. S6.** $^{13}C$ NMR spectrum (100 MHz, $D_2O$, 298 K) of IL-L

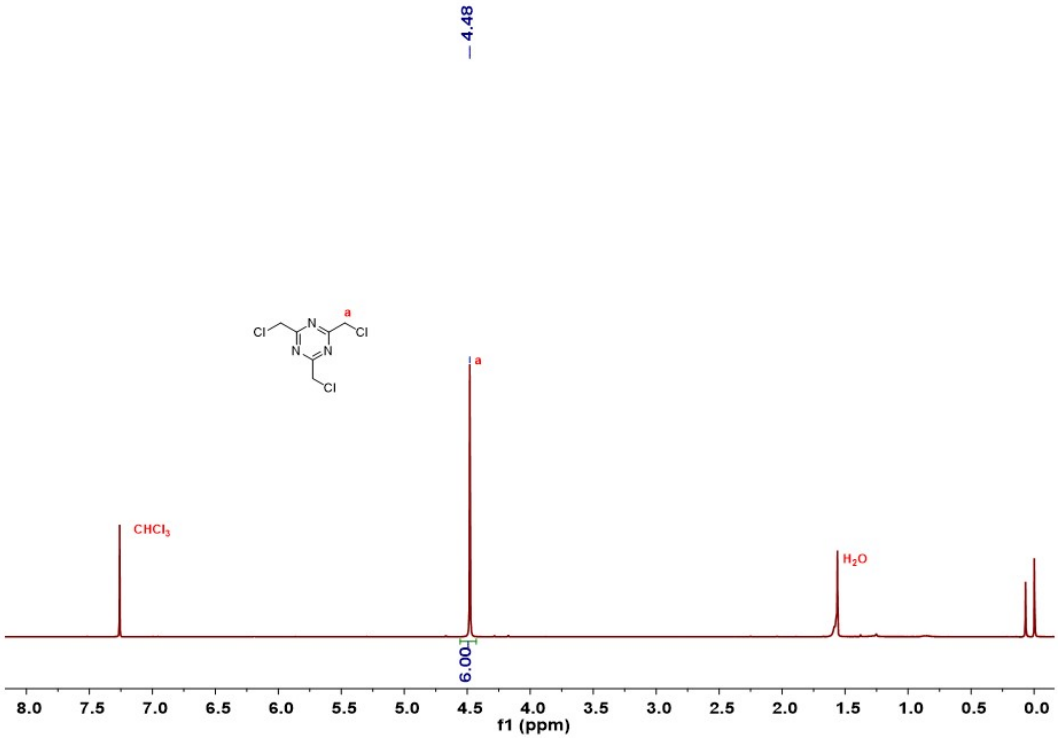


**Fig. S7.** $^{1}H$ NMR spectrum (400 MHz, $CDCl_3$, 298 K) of TBT

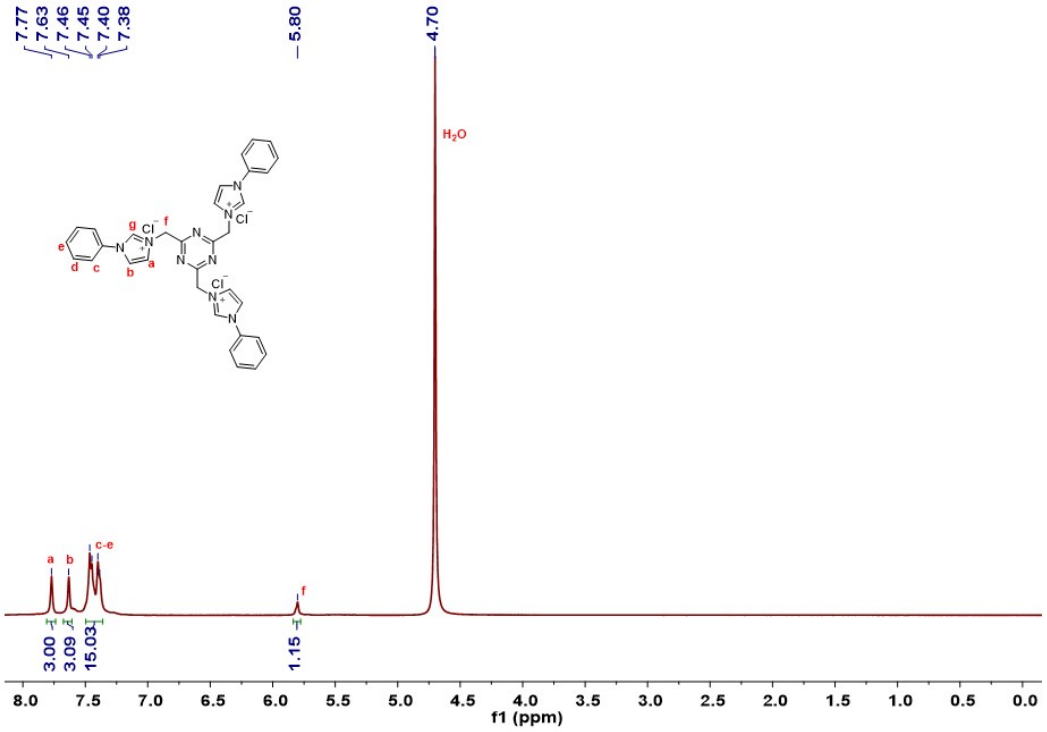


**Fig. S8.** $^{1}$H NMR spectrum (400 MHz, $D_2O$, 298 K) of **M1**

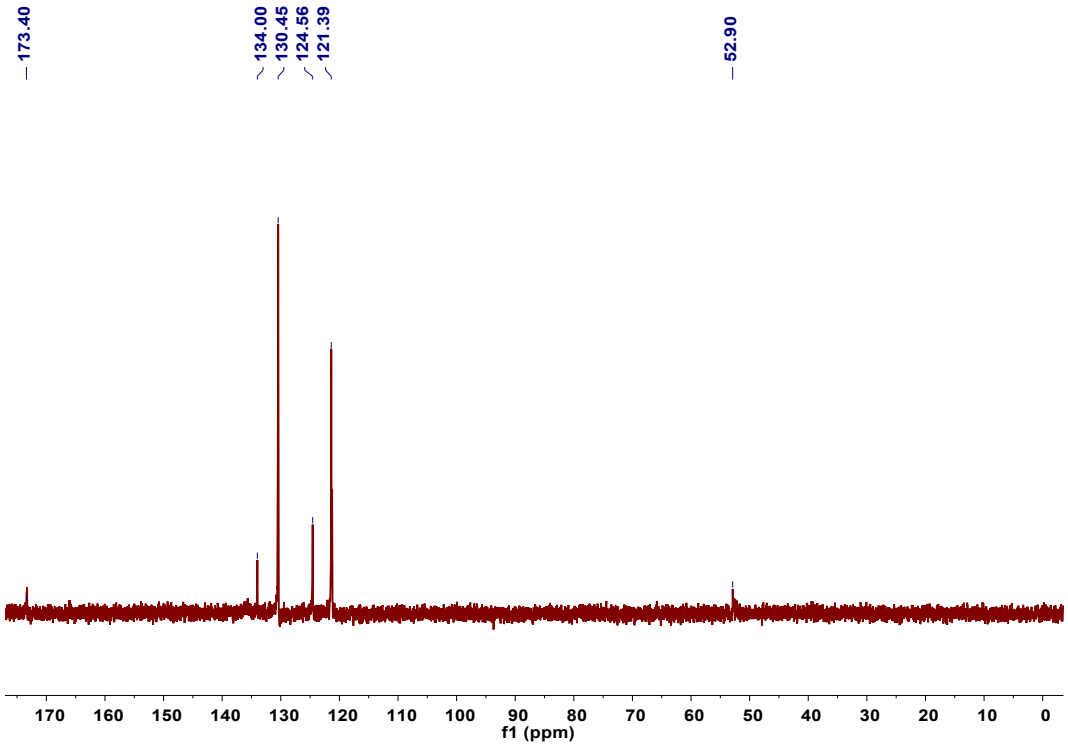


**Fig. S9.** $^{13}$C NMR spectrum (400 MHz, $D_2O$, 298 K) of M1

## 3. Characterization of CTFs

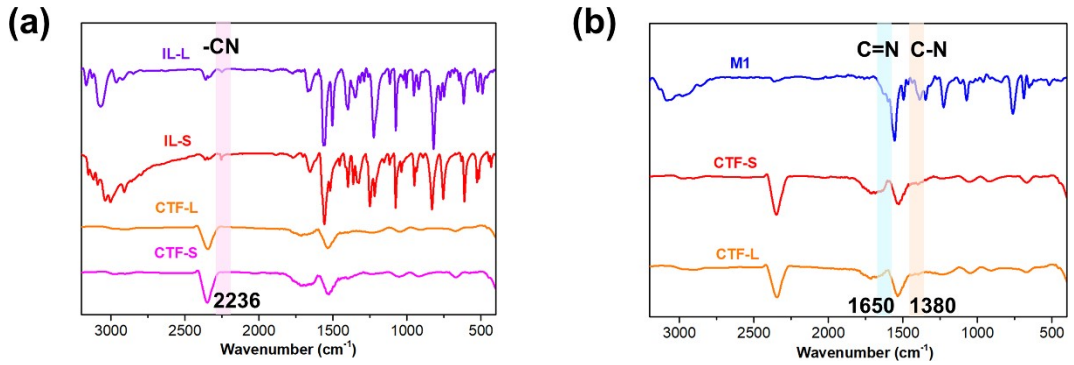


**Fig. S10.** (a) FT-IR spectra of IL-L, IL-S, CTF-L, and CTF-S. (b) FT-IR spectra of M1, CTF-S, and CTF-L.

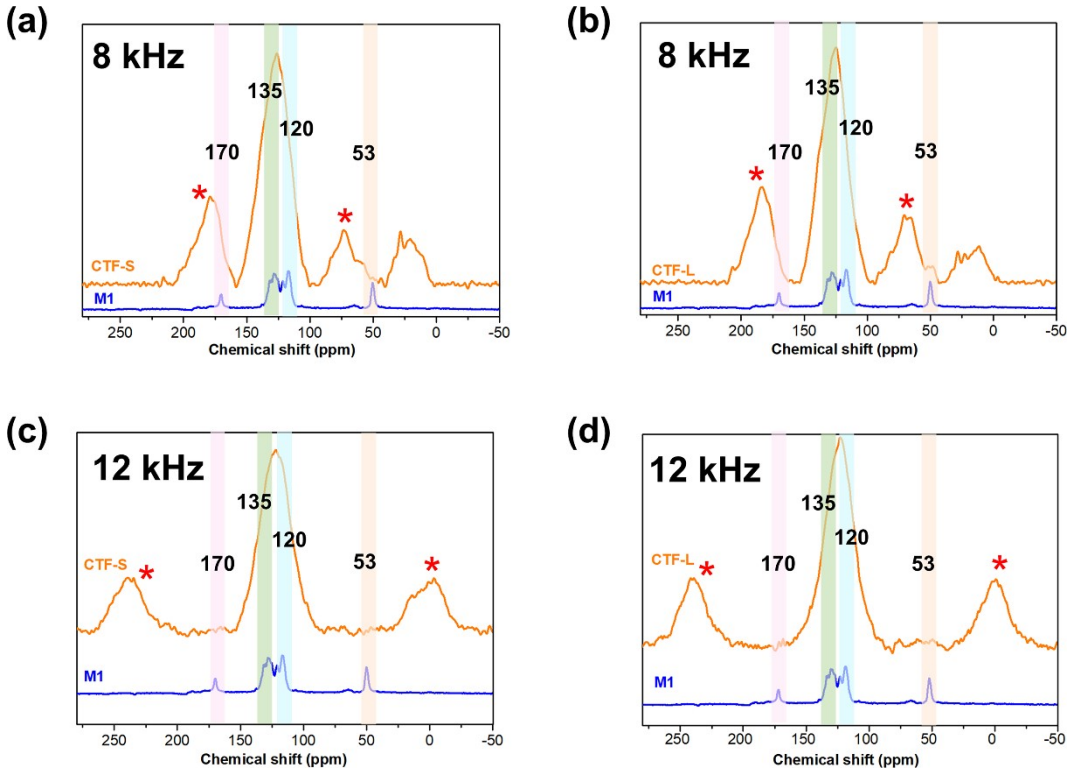


**Fig. S11.** $^{13}C$ CP/MAS NMR spectra of (a) M1 and CTF-S (spinning rate 8 kHz), (b) M1 and CTF-L (spinning rate 8 kHz), (c) M1 and CTF-S (spinning rate 12 kHz), and (d) M1 and CTF-L (spinning rate 12 kHz). * marks spinning sideband.

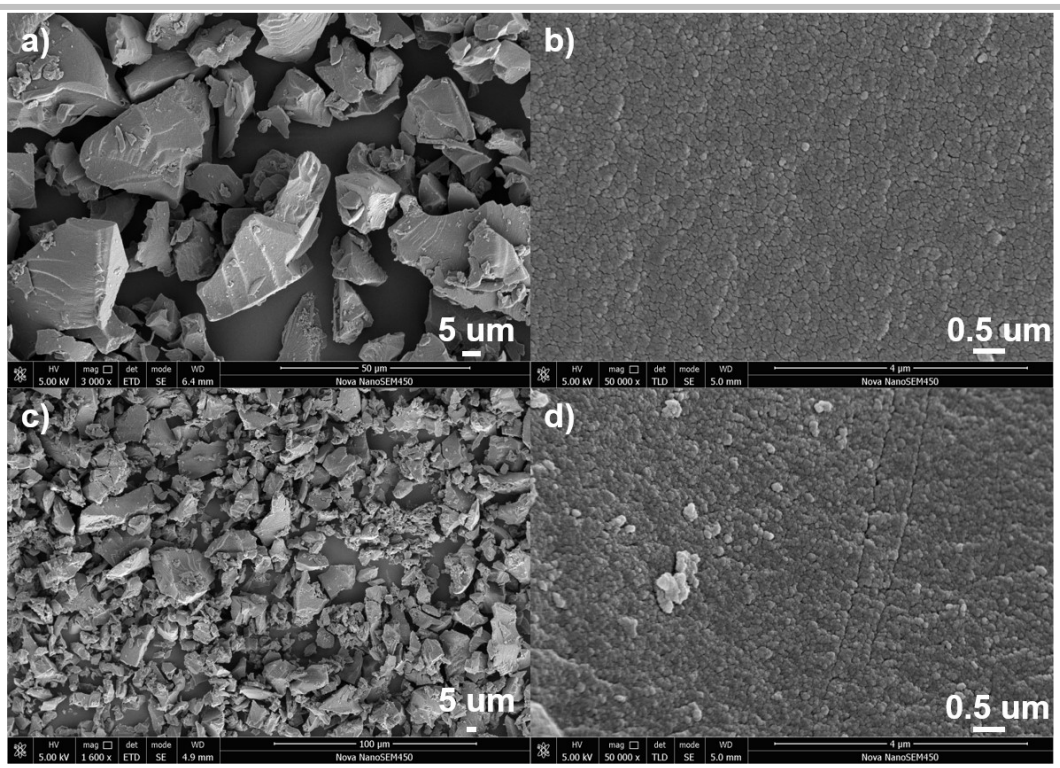


**Fig. S12.** SEM images of CTF-S (a-b) and CTF-L (c-d)

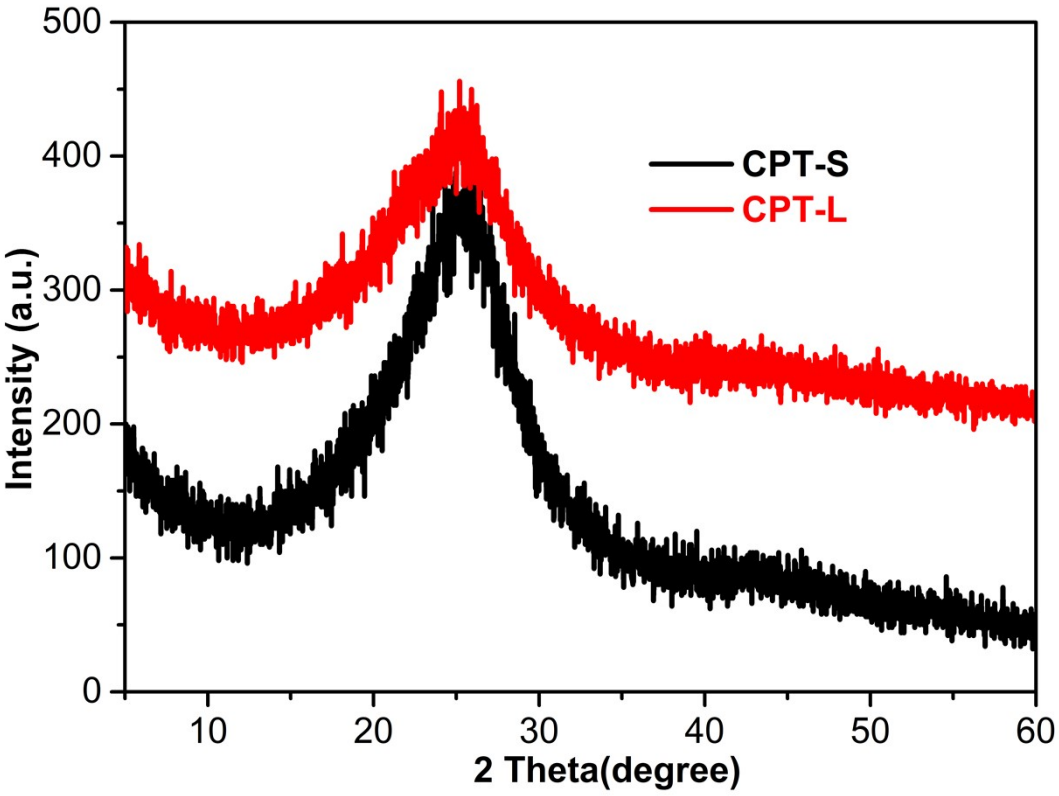


**Fig. S13.** PXRD data of CTF-L and CTF-S

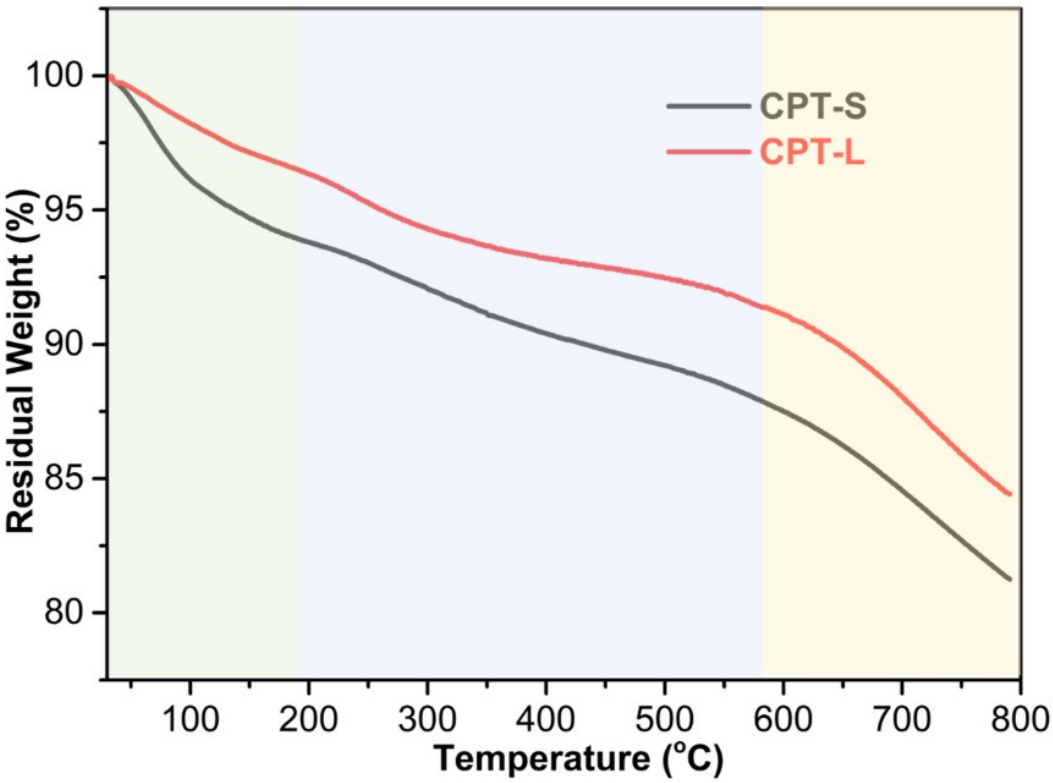


**Fig. S14.** TGA curves for CTF-L and CTF-S

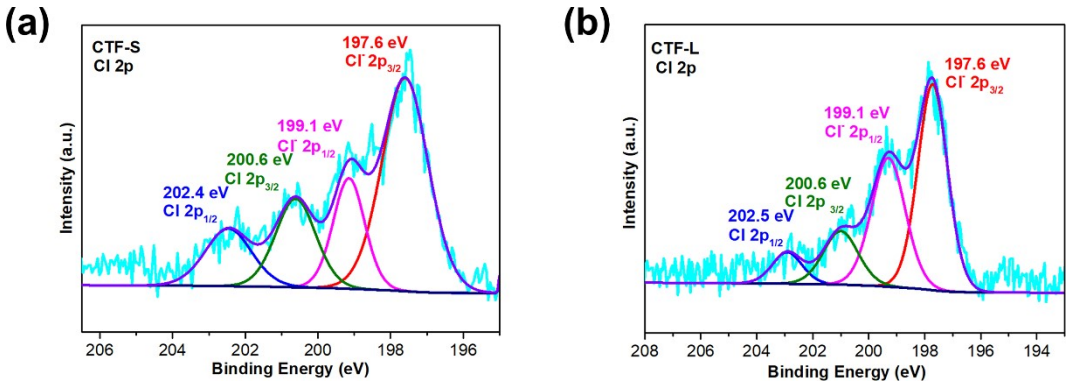


**Fig. S15.** XPS spectra of (a) Cl 2p in CTF-S, (b) Cl 2p in CTF-L

## 4. Palladium sorption

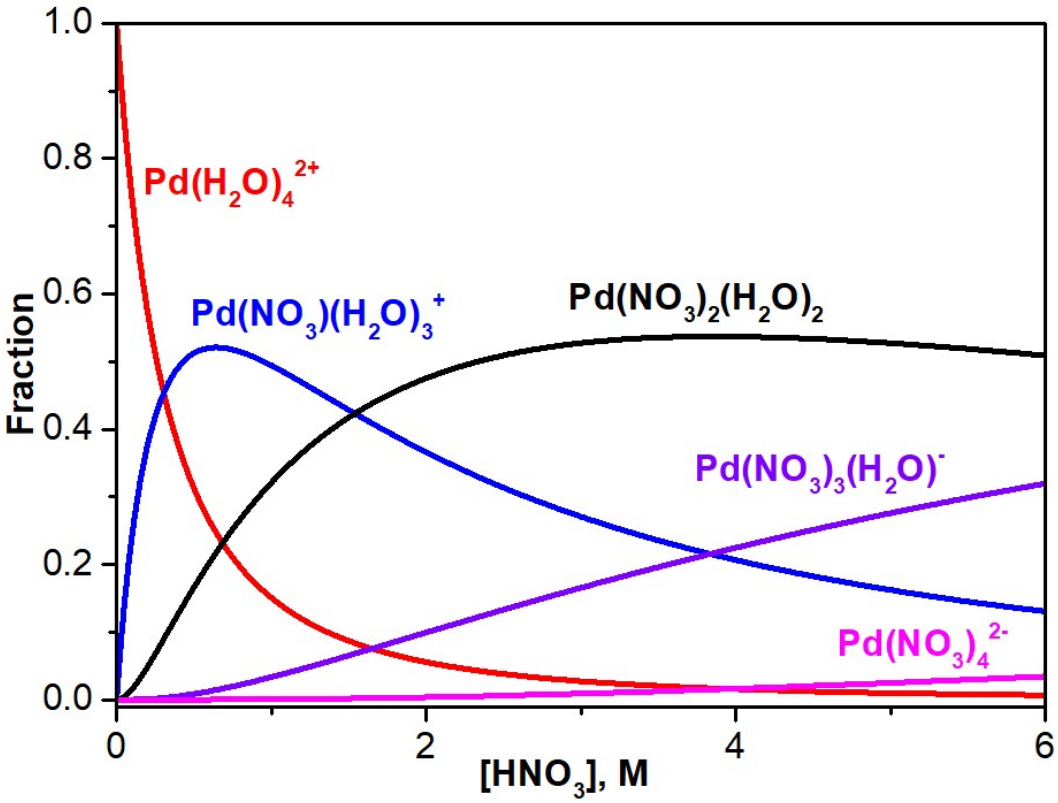


**Fig. S16.** The species distribution of palladium under different concentration of $HNO_3$ conditions.

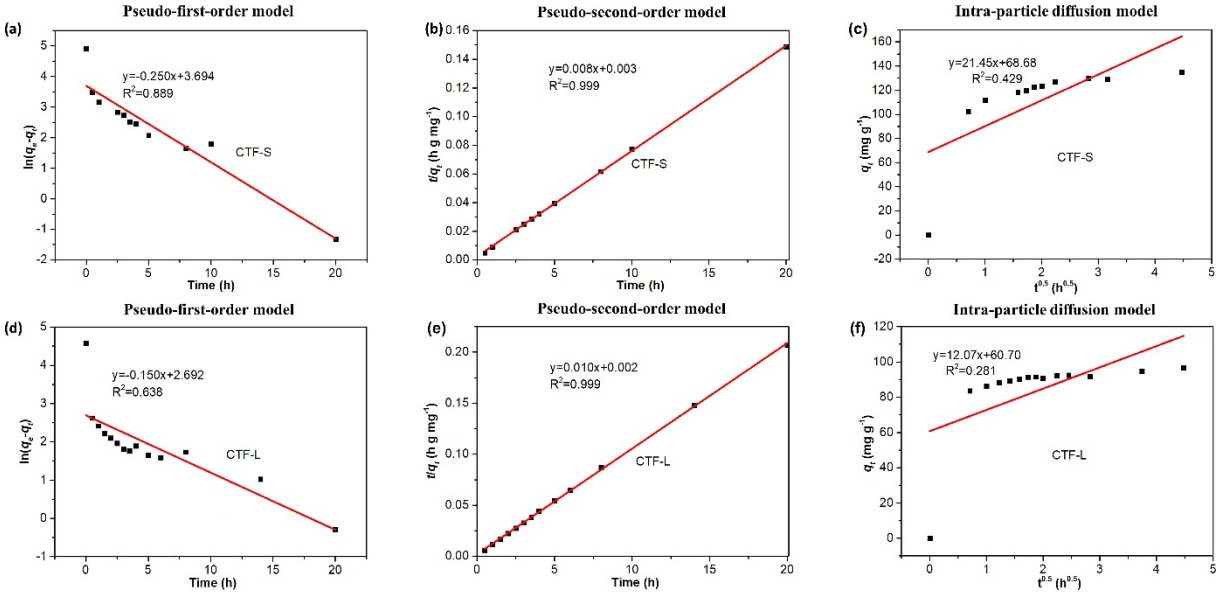


**Fig. S17.** Pseudo-first-order, Pseudo-second-order, and Intra-particle diffusion plots for the palladium sorption onto CTF-L and CTF-S

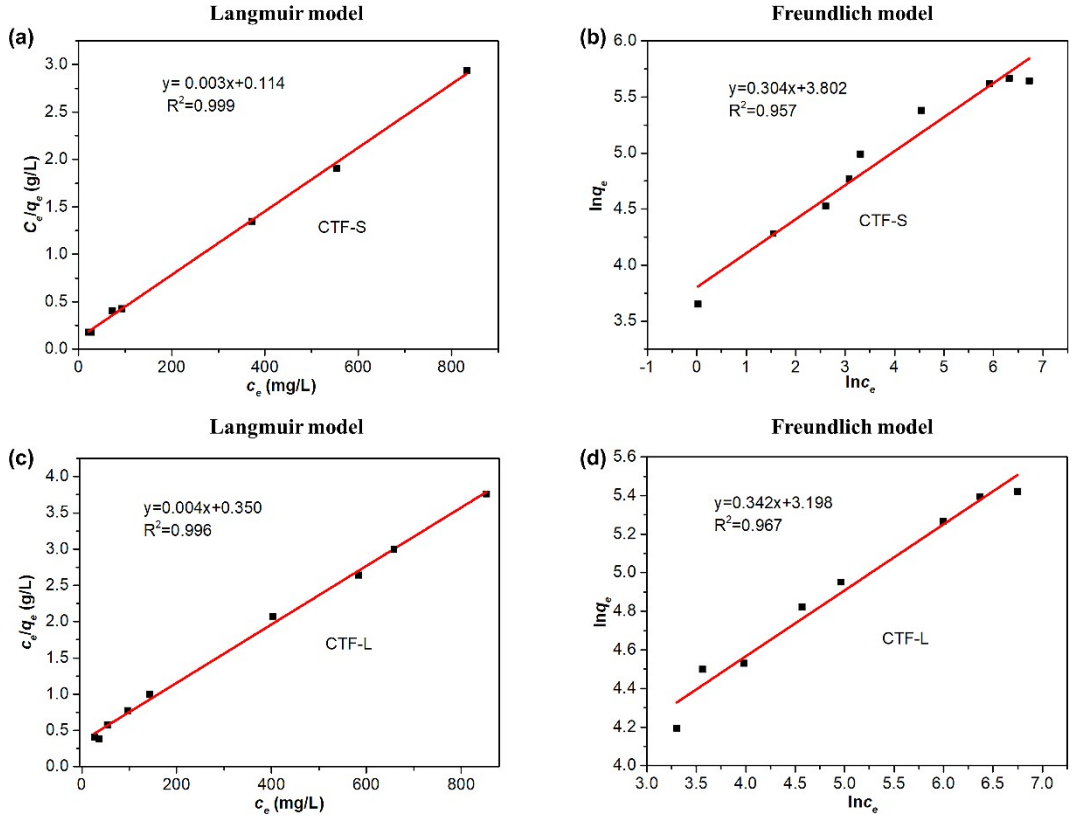


**Fig. S18.** Langmuir and Freundlich model plots for palladium sorption onto CTF-S and CTF-L.

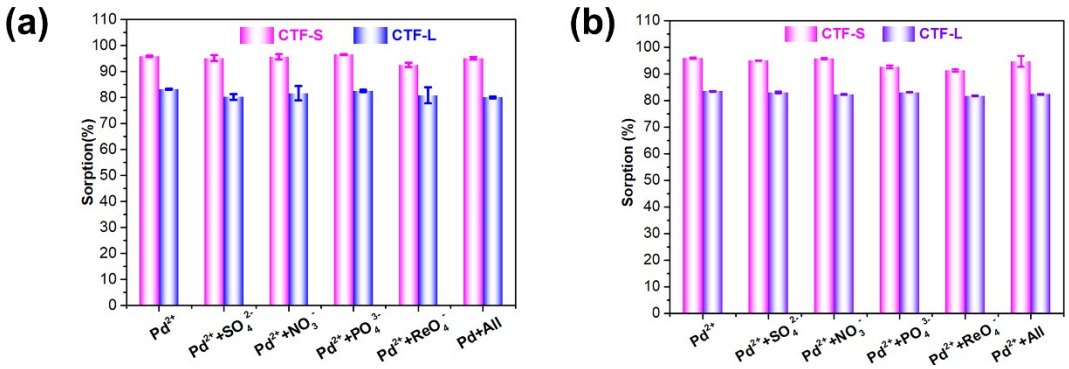


**Fig. S19.** The sorption of palladium in the presence of competitive anions (a) molar ratio (1:1), (b) molar ratio (1:10).

## 5. FT-IR studies of CTFs under different irradiation conditions

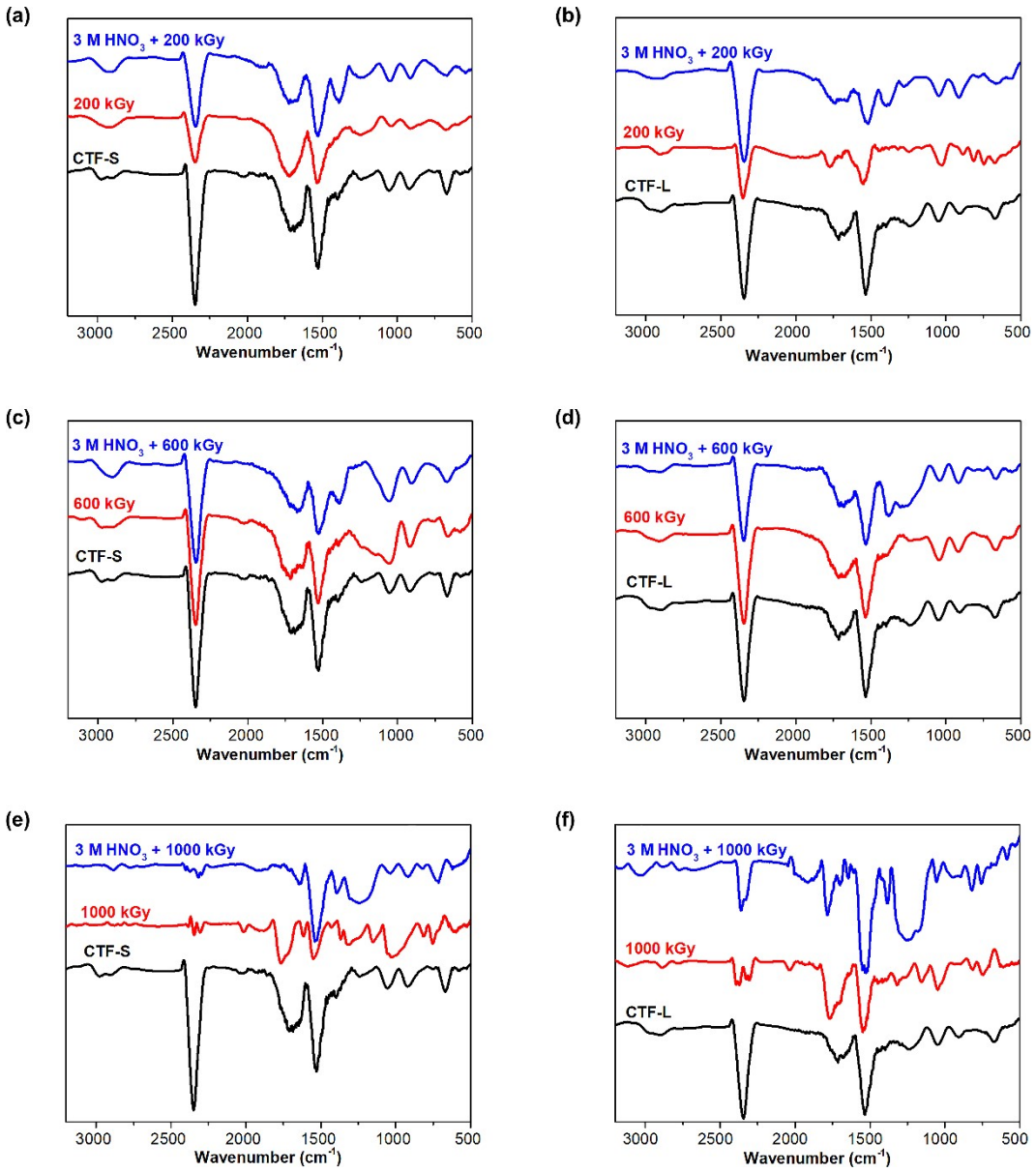


**Fig. S20.** The FT-IR spectra of (a) CTF-S and CTF-S + 3 M $HNO_3$ under 200 kGy, (b) CTF-L and CTF-L + 3 M $HNO_3$ under 200 kGy, (c) CTF-S and CTF-S + 3 M $HNO_3$ under 600 kGy, (d) CTF-L and CTF-L + 3 M $HNO_3$ under 600 kGy, (e) CTF-S and CTF-S + 3 M $HNO_3$ under 1000 kGy, (f) CTF-L and CTF-L + 3 M $HNO_3$ under 1000 kGy.

## 6. Sorption mechanism

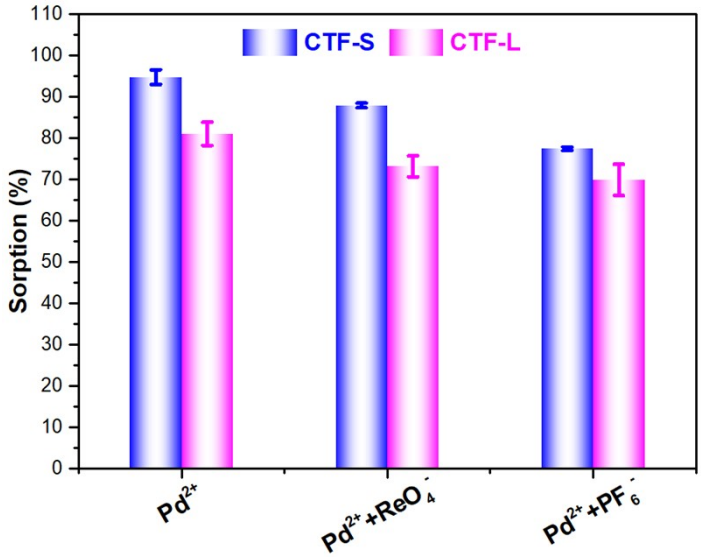


**Fig. S21.** The sorption efficiency of palladium by CTFs in the presence of $ReO_4^-$ and $PF_6^-$ (molar ratio = 1:100, m=15 mg, V=10 mL, $C_{HNO3}$ = 3 M, t=15 h, T=298 K).

## 7. Parameters of kinetics models and isotherm sorption models

**Table S1.** Simulated parameters of CTF-S and CTF-L using different kinetics models

| Model | Parameter | CTF-S | CTF-L |
|---|---|---|---|
| pseudo-first-order model | $q_e$ (mg $g^{-1}$) | 130.1 | 92.4 |
| | $k_1$ ($h^{-1}$) | 0.250 | 0.150 |
| | $q_{e,cal}$ (mg $g^{-1}$) | 40.2 | 14.8 |
| | $R^2$ | 0.889 | 0.638 |
| pseudo-second-order model | $k_2$ ($h^{-1}$) | 0.021 | 0.05 |
| | $q_{e,cal}$ (mg $g^{-1}$) | 125 | 100 |
| | $R^2$ | 0.999 | 0.998 |
| intraparticle diffusion | $k_{int}$ (mg $g^{-1}$ $h^{-0.5}$) | 21.45 | 12.07 |
| | $C$ (mg $g^{-1}$) | 68.68 | 60.70 |
| | $R^2$ | 0.429 | 0.281 |

**Table S2.** Parameters of Langmuir and Freundlich models

| model | parameter | CTF-S | CTF-L |
|---|---|---|---|
| Langmuir | $q_m$ (mg/g) | 286 | 220 |
| | $q_l$ (mg/g) | 333 | 250 |
| | $b_l$ (L/mg) | 0.026 | 0.011 |
| | $R^2$ | 0.999 | 0.996 |
| Freundlich | $n_F$ | 3.290 | 2.924 |
| | $K_F$ ([mg $g^{-1}$ (L $mg^{-1})^{1/n}$] | 44.191 | 24.484 |
| | $R^2$ | 0.957 | 0.967 |

## 8. Comparison of sorption capacity of CTFs with other porous materials

**Table S3.** Comparison of sorption capacity of CTFs for Pd with other porous materials (T=298 K)

| Sorbents | Acidity | Capacity (mg/g) | Refs. |
|---|---|---|---|
| AP-XAD 16 | 3 M $HNO_3$ | 8 | 4 |
| ASUiO-66 | 3 M $HNO_3$ | 45.4 | 5 |
| UiO-66-$NH_2$ | pH=1 | 167 | 6 |
| UiO-66-Pyta | pH=4.5 | 294.1 | 7 |
| IPOF-Cl | pH=7 | 754 | 8 |
| POP-o$NH_2$-Py | pH=7 | 752 | 9 |
| **CTF-S** | **3 M $HNO_3$** | **333** | **This work** |
| **CTF-L** | **3 M $HNO_3$** | **250** | **This work** |

## 9. Composition of simulated HLLW

**Table S4.** Concentrations of the metal ions in simulated HLLW (3 M $HNO_3$)

| Constituent | Conc. (mg/L) | Constituent | Conc. (mg/L) |
|---|---|---|---|
| $Al(NO_3)_3$ | 128.8 | $H_2SeO_3$ | 3.4 |
| $Cd(NO_3)_2$ | 15.3 | $Y(NO_3)_3$ | 156.2 |
| $Ce(NO_3)_3$ | 644 | $ZrO(NO_3)_2$ | 101.4 |
| $La(NO_3)_3$ | 269.5 | $Cr(NO_3)_3$ | 102.6 |
| $Pd(NO_3)_2$ | 216.7 | $Cu(NO_3)_2$ | 21.7 |
| $Ni(NO_3)_2$ | 33.5 | $Sr(NO_3)_2$ | 71.4 |
| $Fe(NO_3)_3$ | 1837.6 | $Mn(NO_3)_2$ | 1185.3 |
| $CsNO_3$ | 450.3 | $NaNO_3$ | 560.8 |
| $Ru(NO)(NO_3)_3$ | 608 | | |

## References

[1] S. Y. Zhang, S. Y. Yang, J. B. Lan, S. J. Yang and J. S. You, *Chem. Commun.*, 2008, 6170-6172.

[2] S. Y. Zhang, J. B. Lan, Z. H. Mao, R. G. Xie and J. S. You, *Growth Des.* 2008., **8**, 3134–3136.

[3] H. Langemheen, V. Korotkovs, J. Bijl, C. Wilson, S. S. Kale, C. Heinis, R. M. J. Liskamp, *ChemBioChem*., 2017, **18**, 387 – 395.

[4] R. Ruhela, K. K. Singh, B. S. Tomar, J. N. Sharma, M. Kumar, R. C. Hubli, A. K. Suri, *Sep. Purif. Technol.,* 2012, **99**, 36-43.

[5] M. Q. Zha, J. Liu, Y.-L. Wong, Z. T. Xu, *J. Mater. Chem. A.,* 2015, 3, 3928–3934.

[6] S. Lin, D. H. Kumar Reddy, J. K. Bediako, M.-H. Song, W. Wei, J.-A. Kim and Y.-S. Yun, *J. Mater. Chem. A.*, 2017, **5**, 13557–13564.

[7] S. Daliran, M. Ghazagh-Miri, A. R. Oveisi, M. Khajeh, S. Navalon, M. Alvaro, M. Ghaffari-Moghaddam, H. Samareh Delarami, and H. García, *ACS Appl. Mater. Interfaces*., 2020, **12**, 25221−25232.

[8] S.-S. Qin, Z.-K. Wang, L. Hu, X.-X. Du, Z. Du, M. Strømme, Q.-F. Zhang, and C. Xu, *Nanoscale.*, 2021, **13**, 3967–3973.

[9] B. Aguila, Q. Sun, H. C. Cassady, C. Shan, Z. Q. Liang, A. M. Al Enizic, A. Nafadyc, J. T. Wright, R. W. Meulenberg, and S. Q. Ma, *Angew. Chem. Int. Ed.* 2020, **59**, 1–6.